IEEE Access
Multidisciplinary | Rapid Review | Open Access Journal

Date of publication xxxx 00, 0000, date of current version xxxx 00, 0000.

*Digital Object Identifier 10.1109/ACCESS.2017.DOI*

# Optimal Linear Controller for Minimizing DC Voltage Oscillations in MMC-Based Offshore Multiterminal HVDC Grids

**ATOUSA ELAHIDOOST [1], (Member, IEEE), LUCA FURIERI [2], (Member, IEEE), MARYAM KAMGARPOUR [3], (Member, IEEE), AND ELISABETTA TEDESCHI [1,4], (Senior Member, IEEE)**

[1]Department of Electric Power Engineering, Norwegian University of Science and Technology, Trondheim 7491, Norway (e-mail: atousa.elahidoost@ntnu.no; elisabetta.tedeschi@ntnu.no)
[2]Laboratoire d'Automatique, EPFL, Lausanne, Switzerland (e-mail: luca.furieri@epfl.ch)
[3]Department of Electrical and Computer Engineering, University of British Colombia, Vancouver, Canada (e-mail: maryamk@ece.ubc.ca), and Automatic Control Laboratory, Department of Information Technology and Electrical Engineering, ETH Zurich, Zurich 8092, Switzerland (e-mail: mkamgar@control.ee.ethz.ch)
[4]Department of Industrial Engineering, University of Trento, Trento, Italy

Corresponding author: Atousa Elahidoost (e-mail: atousa.elahidoost@ntnu.no).

The work of A. Elahidoost and E. Tedeschi was financially supported by the Norwegian Research Council and DNV GL Group under the IDeCON project. The work of L. Furieri and M. Kamgarpour was gratefully supported by the ERC Starting Grant CONENE.

**ABSTRACT** The paper aims at minimizing DC voltage oscillations in offshore multiterminal high-voltage direct current (HVDC) grids based on modular multilevel converters (MMCs). The DC voltage stability is a crucial factor in multiterminal HVDC networks since it is associated with the grid power balance. Furthermore, DC voltage oscillations can cause the propagation of significant disturbances to the interconnected AC grids. This paper proposes an optimal control technique based on semidefinite programming to improve the DC voltage stability margins under the worst-case perturbation scenario. A centralized optimal linear feedback controller is introduced to achieve this goal while ensuring compliance with the control inputs' and state variables' constraints. Furthermore, the methodology is adapted to develop a decentralized optimal linear feedback controller with naturally decoupled constraints on the control inputs and state variables. It is shown that the proposed centralized and decentralized optimal linear controllers can minimize the DC voltage oscillations under the worst-case perturbation scenario in the presence or absence of the droop control gain. The performance of these controllers is verified via eigenvalue stability analysis and time-domain simulations of the MMC-based four-terminal HVDC test grid. Finally, a DC voltage oscillation index is introduced as a potential decision-support criterion. Its applicability is exemplified by identifying, among several options, the HVDC link that gives minimum DC voltage oscillations between independent point-to-point networks while considering the wind intermittency effect.

**INDEX TERMS** DC voltage oscillations, modular multilevel converter, offshore multiterminal HVDC grid, centralized and decentralized optimal linear feedback controller

## I. INTRODUCTION

THE 100% renewable European smart grid cannot be implemented without reliance on wind energy from the offshore wind farms in the North Sea [1]. High-voltage direct current (HVDC) cables are generally used to transfer power from long-distance offshore wind farms to onshore grids at relatively low costs and energy loss [2]. Nowadays, the preferred voltage source converters (VSC) for HVDC applications are modular multilevel converters (MMC) [3]. They are highly efficient and scalable and can produce high-quality voltage and current waveforms with low total harmonic distortion [4].

According to European expansion planning scenarios, the interconnection of the currently existing and newly built offshore point-to-point HVDC grids in the North Sea is inevitable [5], [6]. Implementation of the multiterminal HVDC grid configuration demands control measures to ensure sufficient grid stability margins since such grids were not initially designed to be multiterminal. Thus, improving the DC voltage stability margins is critical to ensure the network's

appropriate performance since DC voltage oscillations can affect the power balance in multiterminal HVDC grids [7]. Moreover, DC voltage oscillations can propagate to connected AC networks due to droop control action [8], [9] and lead to voltage instability and faults, ultimately resulting in blackouts with significant costs [10].

Hence, the paper's primary focus is to minimize the DC voltage oscillations under the worst-case perturbation scenario in multiterminal HVDC grids by an optimal linear feedback controller. This optimal controller improves the DC voltage stability margins to prevent potential critical interactions among different converter stations that may occur due to the interconnection of the point-to-point HVDC grids.

In recent years, most articles on the control of multiterminal HVDC grids apply a droop control strategy. For instance, a strategy for designing DC voltage droop control for multiterminal HVDC systems is presented in [11] while considering the AC and DC grid dynamics. Moreover, a novel adaptive droop control of multiterminal HVDC networks is explained in [12] for frequency regulation and power-sharing. However, the multiterminal HVDC grids analyzed in both articles are based on the 2-level VSCs. Hence, the complexity of the internal control dynamics in MMCs is ignored [3]. In [13], a fuzzy logic-based adaptive droop control in multiterminal HVDC systems for wind power integration is introduced. In this methodology, a compromise between the DC voltage deviation and power-sharing is found for updating the droop gain in an MMC-based HVDC grid. Although MMCs are used, the circulating current's second harmonic is not suppressed through control or modulation, and its potential effects on DC voltage stability and droop gain are not investigated. Reference [14] depicts DC voltage droop control for MMC-based multiterminal HVDC grids. In this technique, the permissible droop gain combinations are not found simultaneously, and are instead selected by successive elimination of those combinations that do not comply with the design constraints.

Within this context, the paper investigates in detail the performance of an analytically derived optimal controller inherently compliant with control inputs' and state variables' constraints, including eigenvalue stability analysis and time-domain simulation. The latter is pivotal in providing physical insights on the action of both centralized and decentralized realizations of the controller. In either case, the controller, which is designed to minimize the DC voltage oscillations under the worst-case perturbation scenario, is successfully applied to an MMC-based four-terminal HVDC grid and proves to work both when modifying the traditional droop control gain and when completely substituting it.

Addressing DC voltage stability under worst-case scenarios without resorting to long time-domain simulations is of high relevance, especially in planning HVDC expansions in AC/DC hybrid networks. Although transmission expansion planning (TEP) problems generally consider cost and loss minimization as the primary objective [15]–[17], grid stability is a prerequisite for any expansion decision. Hence, stability analysis results may prompt reconfiguration of the grid topology or modification of the control parameters to avoid possible contingencies. For instance, reference [18] analyzes the DC voltage stability in AC/DC hybrid microgrids to raise awareness among operators and planners on incorporating this stability study into the planning stage's contingency analysis. To date, few articles have considered stability criteria in the expansion planning of the AC grids. For example, reference [19] implements small-signal stability improvement associated with poorly damped low-frequency electromechanical oscillations in AC power systems' TEP problems. In another work [20], a risk-based TEP analysis implements the transient stability criteria for limiting the synchronous generators' angular swings. A methodology is presented in [21], [22] to determine the optimal grid expansion plan with minimum costs and losses by offering the best AC/DC technology, location, time, and cable routing. However, in this methodology, expansion decisions are made without considering the DC voltage oscillations' effects on AC/DC hybrid grids' cable routing.

Thus, an additional contribution of the paper is to introduce a DC voltage oscillation index that can support grid planners in deciding on the placement of new HVDC links.

It should be noted that the DC voltage oscillations' minimization for the HVDC link placement in multiterminal grids has been studied in our previous works as an initial attempt [23], [24]. However, the HVDC network analyzed was based on simple 2-level VSCs. In addition, the optimal controller's performance was neither evaluated via small-signal eigenvalue stability analysis nor time-domain simulations. We first investigated the challenges associated with MMCs' internal dynamics due to the circulating current in [25] using a centralized optimal controller in a point-to-point configuration. However, the possible MMC effect on DC voltage oscillations in a multiterminal topology was never analyzed. Additionally, in this paper, after investigating the effect of droop gains' variation on the DC voltage stability margins of a four-terminal HVDC grid, the performance of a decentralized optimal controller is evaluated and benchmarked against a centralized one via eigenvalue stability analysis and time-domain simulations.

In summary, the paper's contributions are twofold: First, an optimal linear feedback controller is introduced to minimize the DC voltage oscillations under the worst-case perturbation scenario. This scenario is analytically identified under the grid control inputs' and state variables' physical constraints without the need for long time-domain simulations. The performance of a decentralized optimal controller that can either modify or completely replace the droop control is verified and compared with the centralized one through small-signal eigenvalue stability analysis and time-domain simulations of a four-terminal HVDC grid based on MMCs. Besides, in contrast to the centralized problem formulation, the constraints on the control inputs and state variables are naturally decoupled in the decentralized configuration to ease compliance with the grid codes and standards. Second, the

DC voltage oscillation index as a decision support criterion is used to find the best HVDC link placement to connect two independent MMC-based HVDC links into a multiterminal grid while considering the wind intermittency effect.

The rest of the paper is organized as follows: Section II presents the optimal control problem for minimizing DC voltage oscillations under the worst-case perturbation scenario. A tractable formulation of the problem based on semidefinite programming (SDP) is given for the centralized and decentralized optimal linear feedback controllers. Section III introduces an MMC-based four-terminal offshore HVDC grid as the reference test case. The grid's state-space model is a prerequisite for the optimal control problem formulation, and it is developed and validated through time-domain simulations. Small-signal eigenvalue stability analysis is performed to study the system's dynamics and stability margins for the test grid in section III.C, which is then used to validate the optimal controller performance. Finally, case studies and time-domain simulation results, including the application of the DC voltage oscillation index, are given in section IV, followed by the conclusion in section V.

## II. OPTIMAL CONTROL PROBLEM

The optimal control methodology finds the worst-case perturbation scenario and acts upon the system eigenvalues to reduce the DC voltage oscillations via an optimal linear feedback controller. The proposed centralized optimal controller is inspired by the approach presented in [26], which evaluates the placement of HVDC links for AC grid reinforcement by minimizing the generator frequency deviations. We have adapted this approach to our objective to reduce the DC voltage oscillations in MMC-HVDC networks.

In the centralized configuration, any entry of the optimal controller matrix can arbitrarily be assigned a value by the optimization procedure. Besides, the set of possible perturbations is subject to a single high-dimensional ellipsoidal constraint. Afterward, a decentralized optimal controller is introduced. In the decentralized configuration, the optimal controller matrix is block-diagonal to match the grid sparsity pattern. Hence, there is no need for communication between converter stations, and only the local state information is needed. Moreover, constraints on the control inputs and state variables are naturally decoupled, which allows for more flexibility and realism in the design. The preliminary formulation of the decentralized methodology was reported in our previous work [24]. However, the feasibility and applicability of the controller had not yet been studied. Therefore, in this paper, the optimal controller is realized in MMC-based multiterminal HVDC grids. Its performance is verified in detail via small-signal eigenvalue stability analysis and time-domain simulations.

### A. PROBLEM STATEMENT

The optimal DC voltage oscillation index, $J_{osci}$, is stated as a min-max optimization problem:

$$J_{osci} = \min_{K} \max_{x(0)\in\mathbb{X}_0} \int_0^\infty z(t)^T z(t)\, dt \tag{1}$$

$$s.t. \quad \dot{x}(t) = Ax(t) + Bu(t) \tag{2}$$

$$z(t) = Cx(t) \tag{3}$$

$$u(t) = Kx(t) \tag{4}$$

where $x$, $u$, and $z$ are defined as the grid state vector, control input vector, and output vector, respectively.

In the case $K$ is centralized, (1) is subject to:

$$x(0) \in \mathbb{X}_0 = \{x \in \mathbb{R}^n : x^T E_x x \leq 1\} \tag{5}$$

$$u(t) \in \mathbb{U} \ = \{u \in \mathbb{R}^m : u^T E_u u \leq 1\} \tag{6}$$

or in the case $K$ is decentralized, (1) is subject to:

$$x(0) \in \mathbb{X}_0 = \{x_i \in \mathbb{R}^{n_i} \ : \forall i \in \mathbb{Z}_{[1,r]} \ x_i^T E_x^i x_i \leq 1\} \tag{7}$$

$$u(t) \in \mathbb{U} \ = \{u_j \in \mathbb{R}^{m_j} : \forall j \in \mathbb{Z}_{[1,q]} \ u_j^T E_u^j u_j \leq 1\} \tag{8}$$

The objective is to minimize the desired signals' oscillations, $z$, being the grid DC voltages. Parameters $n$ and $m$ are the number of grid state variables and control inputs, respectively. The control inputs are the reference parameters of the grid converters' control loops, further explained in section III. Matrices $A \in \mathbb{R}^{n\times n}$, $B \in \mathbb{R}^{n\times m}$, and $C \in \mathbb{R}^{n\times n}$ are the grid state-space matrices. The matrix $K \in \mathbb{R}^{m\times n}$ is the grid optimal linear feedback controller, which minimizes the DC voltage oscillations under the worst-case perturbation scenario $\mathbb{X}_0$. Problem (1) is subject to constraints on $x(0)$ and $u(t)$. Typically, the constraints have the form (5)-(6), and the controller matrix $K$ is allowed to be centralized. In this case, the matrices $E_x > 0$, and $E_u > 0$, are symmetric positive definite and define the ellipsoidal constraints on the state variables and control inputs. Namely, the constraint on the initial states' perturbations (5) confines the sum of the squares of the disturbances on the state variables of the MMC terminals and HVDC cables (e.g., MMC AC-side and DC-side currents, zero-sequence circulating currents, DC-side voltages, zero-sequence energy sums, and the integral states associated with the PI controllers). Similarly, (6) constrains the sum of the squares of the control inputs, including references for the DC-side voltages, active and reactive powers, and zero-sequence energy sums. To improve the centralized problem formulation's shortcomings, the decentralized optimal controller $K$ is proposed, which does not require communication between the different converter stations. Besides, to enhance the constraints' flexibility and their physical sensibility, the possibility of decoupling of the initial states' perturbations and control inputs' constraints for every converter station is implemented in the decentralized problem formulation as given in (7)-(8). Accordingly, $r$ and $q$ are defined as the number of the ellipsoidal constraints for the grid state variables and control inputs, respectively. Thus, $\sum_{i=1}^{r} n_i = n$, and $\sum_{j=1}^{q} m_j = m$. The paper will treat

both centralized and decentralized scenarios and verify their performance through eigenvalue stability analysis and time-domain simulations.

### B. PROBLEM FORMULATION

The proposed optimal control problem is non-convex in its cost function and constraints, and it is not easy to directly compute the optimal solution. As we show in the following subsections, the problem can be approximated to a convex SDP formulation using linear matrix inequalities (LMIs) [27].

#### 1) Centralized Optimal Linear Feedback Controller

In the centralized problem formulation, the optimal controller $K$ is found by solving (1)-(6). The architecture of the centralized optimal linear feedback controller is shown in Fig. 1a. The non-convex min-max optimization problem can be converted to an SDP problem using the Lyapunov stability interpretation and LMI theory, as shown in [26]. It is worth mentioning that [26] focuses on the generator frequency deviations' minimization in AC grids. In contrast, this paper's goal is to minimize the DC voltage oscillations in HVDC grids. We have previously investigated the performance of the adapted centralized optimal controller in an MMC-based point-to-point configuration [25]. However, its performance in multiterminal grids has never been studied. Hence, the adapted centralized optimal controller formulation is presented here as a benchmark and is verified via small-signal eigenvalue stability analysis and time-domain simulations of an MMC-based offshore four-terminal HVDC grid.

The optimal DC voltage oscillation index under the worst-case perturbation scenario is approximated as follows such that $J_{osci} \leq \tilde{J}_{osci}$:

$$\frac{1}{\tilde{J}_{osci}} = \max_{s>0,\, Q>0,\, Y} s \tag{9}$$

$$s.t. \quad \begin{bmatrix} (AQ+BY)+(AQ+BY)^T & QC^T \\ CQ & -I \end{bmatrix} \leq 0 \tag{10}$$

$$\begin{bmatrix} Q & Y^T \\ Y & sE_u^{-1} \end{bmatrix} \geq 0 \tag{11}$$

$$Q - sE_x^{-1} \geq 0 \tag{12}$$

where $s>0$ is a scalar quantity whose inverse represents the upper bound of the DC voltage oscillations. Specifically, it can be seen that $x(t)^T P x(t)$ with $P=Q^{-1}$ is a closed-loop Lyapunov function and that the centralized optimal linear feedback controller is recovered as $K=YQ^{-1}$. Furthermore, the corresponding worst-case perturbation scenario $x_{0,worst}$ is retrieved as $\hat{E}^{-T}v_1$, where $\hat{E}=VD^{1/2}$, $V$ contains the eigenvectors of $E_x$, $D$ is diagonal with the eigenvalues of $E_x$, and $v_1$ is the eigenvector of $\hat{E}^{-1}Q^{-1}\hat{E}^{-T}$ associated with its largest eigenvalue.

The globally optimal cost $\tilde{J}_{osci}$ is therefore tightly approximated by maximizing (9) subject to (10)-(12). Out of the three inequality constraints, the first one (10) implements the Lyapunov stability criteria. The second (11) and third (12) ones are concerned with the confinement of the system control inputs and the state variables in ellipsoidal constraints encoding their physical restrictions. Such an ellipsoidal constraint limits the grid maximum voltages and currents within a range by exploiting the $E_u > 0$, and $E_x > 0$ matrices to define their maximum permissible variation.

#### 2) Decentralized Optimal Linear Feedback Controller

In contrast to the centralized controller, the decentralized optimal linear feedback controller matrix can have the desired sparsity pattern that is block-diagonal, as shown in Fig. 1b. By assuming a block-diagonal configuration of the controller $K$, each block corresponds to a converter station, and all inter-converter entries are zero. Hence, there is no need for data communication between converter stations, resulting in a more reliable solution at the potential cost of lower performance. In the decentralized formulation, the constraints on the initial states' perturbations and control inputs for every converter station are decoupled, which is physically more practical. The SDP formulation of the decentralized optimal control problem stated in (1)-(4), (7), and (8) was preliminarily given in our previous work [24], and its derivation is recalled in the following for completeness with the final formulation result presented in (27)-(33). Moreover, the applicability and performance of the controller in an MMC-based multiterminal HVDC grid had never been investigated. Hence, this gap is filled in the following by eigenvalue stability analysis and time-domain simulations.

Formulation of the worst-case oscillation: According to the Lyapunov stability theory, if $(A+BK)$ is asymptotically stable, then the quadratic integral of (1) can be written as:

$$\int_0^\infty x(t)^T C^T C x(t)\, dt = x(0)^T P x(0) \tag{13}$$

where $P > 0$ is the symmetric positive definite unique solution of the $P(A+BK)+(A+BK)^T P+C^T C=0$.

Since $E_x^i > 0$, $\forall i \in \mathbb{Z}_{[1,r]}$, then:

$$E_x^i = \hat{E}_x^i \hat{E}_x^{iT}, \quad \hat{E}_x^i = V_x^i D_x^{i\frac{1}{2}} \tag{14}$$

where $V_x^i$ contains the eigenvectors of $E_x^i$ and $D_x^{i\frac{1}{2}}$ holds the square root of the $E_x^i$ eigenvalues on its diagonal. Vector $\tilde{x}_i$ is defined such that $x_i = (\hat{E}_x^i)^{-T}\tilde{x}_i$.

Matrix $P$ is needed to be block-diagonal with dimensions $n_i \times n_i$ on its i-th block $P_i$ in order to be able to generate an optimal controller $K$ with the desired block-diagonal sparsity pattern and to decouple the initial disturbances into separate ellipsoids. Therefore:

$$\begin{aligned} &\max_{x(0)\in\mathbb{X}_0} x(0)^T P x(0) \\ &= \sum_{i=1}^{r} \max_{||\tilde{x}_i||_2 \leq 1,\, \forall i \in \mathbb{Z}_{[1,r]}} \tilde{x}_i^T (\hat{E}_x^i)^{-1} P_i (\hat{E}_x^i)^{-T} \tilde{x}_i \\ &= \sum_{i=1}^{r} \lambda_{max}((\hat{E}_x^i)^{-1} P_i (\hat{E}_x^i)^{-T}) \end{aligned} \tag{15}$$

This article has been accepted for publication in a future issue of this journal, but has not been fully edited. Content may change prior to final publication. Citation information: DOI 10.1109/ACCESS.2021.3096291, IEEE Access



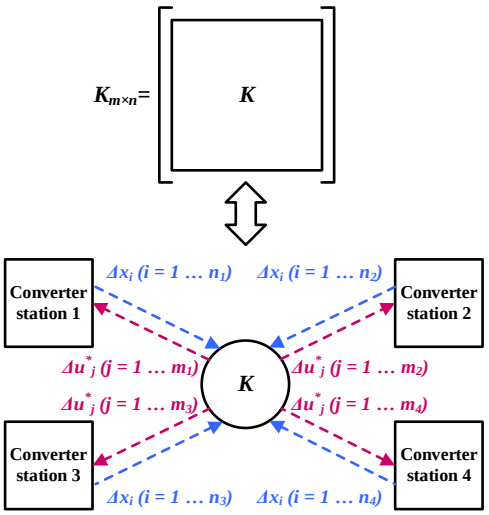


(a) Centralized optimal linear feedback controller architecture.

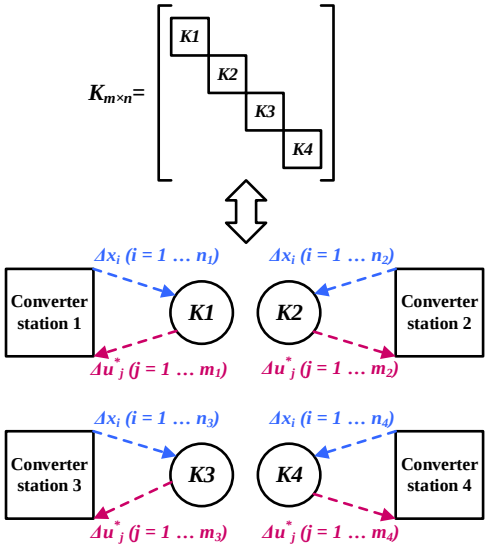


(b) Decentralized (block-diagonal) optimal linear feedback controller architecture.

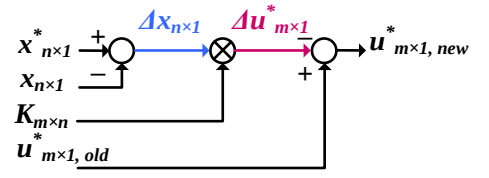


$\Delta x_{\text{Converter station 4}} = [\Delta i_{v,d4}\ \Delta i_{v,q4}\ \Delta \xi_{ivd4}\ \Delta \xi_{ivq4}\ \Delta i_{cc,z4}\ \Delta \xi_{iccz4}\ \Delta v_{dc4}\ \Delta \xi_{Pac4}\ \Delta \xi_{Qac4}\ \Delta w_{\Sigma,z4}\ \Delta \xi_{w\Sigma z4}\ \Delta i_{c1,14}\ \Delta i_{c2,14}\ \Delta i_{c3,14}\ \Delta i_{c1,24}\ \Delta i_{c2,24}\ \Delta i_{c3,24}]$

$\Delta u^*_{\text{Converter station 4}} = [\Delta v^*_{dc4}\ \Delta P^*_{ac4}\ \Delta Q^*_{ac4}\ \Delta w^*_{\Sigma,z4}]$

(c) Centralized/decentralized optimal controller implementation.

**FIGURE 1.** Centralized/decentralized optimal linear feedback controllers' architecture and implementation. Every converter station is composed of an MMC and connected HVDC cables. State variables and control inputs are marked in blue and red, respectively.

Then, (15) can be substituted in (1) resulting in:

$$\begin{aligned} &\min_{K} \sum_{i=1}^{r} \lambda_{max}((\hat{E}_x^i)^{-1} P_i (\hat{E}_x^i)^{-T}) \\ &s.t. \quad P(A+BK)+(A+BK)^T P + C^T C = 0 \end{aligned} \tag{16}$$

Next, $s_i > 0,\ \forall i \in \mathbb{Z}_{[1,r]}$ can be defined such that:

$$\lambda_{max}((\hat{E}_x^i)^{-1} P_i (\hat{E}_x^i)^{-T}) \leq \frac{1}{s_i} \tag{17}$$

Equation (17) is equivalent to:

$$Q_i - s_i (E_x^i)^{-1} \geq 0 \tag{18}$$

where $Q_i \geq 0$, $Q_i = (P_i)^{-1}$, $\forall i \in \mathbb{Z}_{[1,r]}$, and $Q$ is defined to be block-diagonal such that $Q = \text{blkdiag}(Q_i)$.

Therefore, by exploiting the Schur complement and defining the new variable $Y = KQ$, (16) can be formulated as follows:

$$\begin{aligned} &\min_{s_i,\, Q_i \geq 0,\, Y} \sum_{i=1}^{r} \frac{1}{s_i} \\ &s.t. \qquad Q_i - s_i (E_x^i)^{-1} \geq 0,\ \forall i \in \mathbb{Z}_{[1,r]} \\ &\qquad \begin{bmatrix} (AQ+BY)+(AQ+BY)^T & QC^T \\ CQ & -I \end{bmatrix} \geq 0 \end{aligned} \tag{19}$$

Robustness to initial states' perturbations: Considering (4), (7), and (8), the control inputs should comply with $u_j^T(t) E_u^j u_j(t) \leq 1,\ \forall j \in \mathbb{Z}_{[1,q]}$ at any time instant $t \in \mathbb{R}_0^+$, that $u_j(t) = K_j x(t)$, and $K = \text{blkcol}(K_j)$. Namely, $x(t)^T K_j^T E_u^j K_j x(t) \leq 1,\ \forall j \in \mathbb{Z}_{[1,q]}$ should hold at any time instant $t \in \mathbb{R}_0^+$. Since $P$ can also be interpreted as level sets for the state variables' trajectories, once it satisfies $x(t_1)^T P x(t_1) \leq k$ for some $k > 0$ at time instant $t_1 \in \mathbb{R}_0^+$, it can also be valid for any time instant $t > t_1$. Hence:

$$x(0)^T P x(0) \leq \max_{x(0)\in \mathbb{X}_0} x(0)^T P x(0) \leq \sum_{i=1}^{r} \frac{1}{s_i} \tag{20}$$

where (20) can also be given as $x(0)^T \frac{P}{\sum_{i=1}^{r} \frac{1}{s_i}} x(0) \leq 1$.

Thus, the control input constraints can be written as:

$$K_j^T E_u^j K_j \leq \frac{P}{\sum_{i=1}^{r} \frac{1}{s_i}},\ \forall j \in \mathbb{Z}_{[1,q]} \tag{21}$$

where (21) is equivalent to $Q - Y_j^T E_u^j \sum_{i=1}^{r} \frac{1}{s_i} Y_j \geq 0$.

Therefore, by using the Schur complement, the former can be formulated as below:

$$\begin{bmatrix} Q & Y_j^T \\ Y_j & (E_u^j)^{-1} (\sum_{i=1}^{r} \frac{1}{s_i})^{-1} \end{bmatrix} \geq 0,\ \forall j \in \mathbb{Z}_{[1,q]} \tag{22}$$

It should be noted that if $r = 1$, then (22) is a SDP constraint, and the problem of (19), and (22) entails a convex formulation by maximizing $s$ instead of minimizing $\frac{1}{s}$. However, if $r > 1$, then further elaboration is required to obtain a convex problem formulation.

Convex problem formulation: The harmonic mean of $s_i > 0$, $\forall i \in \mathbb{Z}_{[1,r]}$ is defined as:

$$h(s) = \frac{r}{\sum_{i=1}^{r} \frac{1}{s_i}} \tag{23}$$

Then, a new decision variable $w$ is defined such that $w \leq h(s)$, and (23) accordingly becomes:

$$\sum_{i=1}^{r} \frac{w^2}{s_i} \leq rw \tag{24}$$

Next, a set of decision variables $y_i$, $\forall i \in \mathbb{Z}_{[1,r]}$ is introduced to cast (24) as follows:

$$w^2 \leq s_i y_i, \quad \sum_{i=1}^{r} y_i = rw, \quad \forall i \in \mathbb{Z}_{[1,r]} \tag{25}$$

Thus, (25) can be written as the second-order cone programming constraint:

$$\left\| \begin{matrix} 2w \\ s_i - y_i \end{matrix} \right\|_2 \leq s_i + y_i, \quad \forall i \in \mathbb{Z}_{[1,r]} \tag{26}$$

Therefore, a tractable SDP formulation of the decentralized optimal control problem can be obtained as follows:

$$\frac{1}{\tilde{J}_{osci}} = \max_{s_i>0,\, Q_i>0,\, Y,\, w,\, y_i} w \tag{27}$$

$$s.t. \quad \begin{bmatrix} (AQ+BY)+(AQ+BY)^T & QC^T \\ CQ & -I \end{bmatrix} \leq 0 \tag{28}$$

$$\begin{bmatrix} Q & Y_j^T \\ Y_j & \frac{w}{r}(E_u^j)^{-1} \end{bmatrix} \geq 0, \quad \forall j \in \mathbb{Z}_{[1,q]} \tag{29}$$

$$Q_i - s_i (E_x^i)^{-1} \geq 0, \quad \forall i \in \mathbb{Z}_{[1,r]} \tag{30}$$

$$\left\| \begin{matrix} 2w \\ s_i - y_i \end{matrix} \right\|_2 \leq s_i + y_i, \quad \forall i \in \mathbb{Z}_{[1,r]} \tag{31}$$

$$\sum_{i=1}^{r} y_i = rw, \quad Q = \text{blkdiag}(Q_i) \tag{32}$$

$$Y = \text{blkcol}(Y_i), \quad Y \text{ is decentralized.} \tag{33}$$

Equations (29) and (30) are representative of the separate ellipsoidal inequality constraints on the control inputs and state variables, respectively. Namely, the decentralized formulation can define different inequality constraints for every converter station based on their maximum permissible voltages and currents.

## III. STATE-SPACE MODEL OF THE MMC-BASED OFFSHORE MULTITERMINAL HVDC GRID

The four-terminal offshore HVDC grid shown in Fig. 2 is based on the HVDC grids' test system proposed in [28] whose model parameters are reported in Table 1. We are interested in studying the interconnection of two independent point-to-point HVDC links between offshore wind farms and onshore power grids (MMC1 to MMC3 and MMC2 to MMC4). Hence, the test grid is adapted to resemble a real case, i.e., with actual wind speed time series and distances

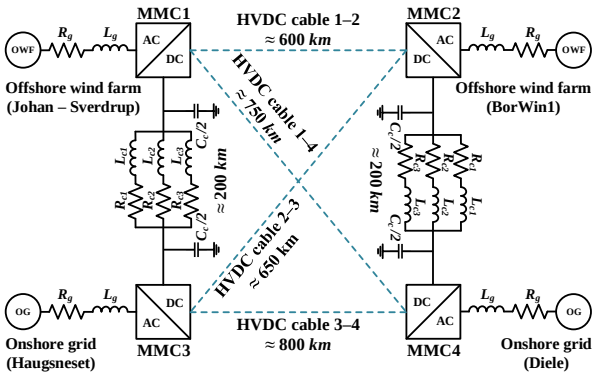


**FIGURE 2.** Offshore four-terminal HVDC grid topology. Dashed blue lines are the potential HVDC link expansion routes.

between the locations. The two selected offshore locations in the North Sea are BorWin1 (Germany) and Johan-Sverdrup (Norway). BorWin1 is already an HVDC-connected wind farm, while Johan-Sverdrup is currently an HVDC-connected oil and gas platform. However, Utsira High, where Johan-Sverdrup is located, has been identified as a potential offshore wind site in Norway [29]. The choice between the four potential expansion routes (shown as dashed blue lines in Fig. 2) considers their different stabilizing effects on the multiterminal HVDC grid.

In the following subsections, the test grid steady-state time-invariant (SSTI) state-space model is obtained and validated as a prerequisite for the small-signal eigenvalue stability analysis. This analysis serves two purposes: First, to obtain the $A \in \mathbb{R}^{n\times n}$, $B \in \mathbb{R}^{n\times m}$, and $C \in \mathbb{R}^{n\times n}$ matrices required for the optimal control formulation defined in section II to minimize the DC voltage oscillations of the four-terminal HVDC grid under the worst-case perturbation scenario. Second, to obtain a greater insight into the grid dynamics and stability margins, dependent on the modeling and control parameters. Together with time-domain simulations, the eigenvalue analysis results are then used to corroborate the performance of the optimal linear feedback controller.

### A. STATE-SPACE REPRESENTATION OF THE MMC

The SSTI model of the MMC (shown in Fig. 3) is developed according to the simplified zero-sequence model with reduced order, which originates from the energy-based representation of the converter with compensated modulation (CM) [30]. In the energy-based formulation, the sum of the upper and lower arm capacitor energy is defined as the converter state variable along with the other states. Unlike the uncompensated modulation, the CM-based implementation allows for compensation of the arm capacitor voltages' oscillations in the converter without further control loops. The simplified zero-sequence model with reduced order is an attractive solution for large-scale power system stability studies. Its adequate fidelity is proven in [30]. In the simplified model, the *dq*-components of the MMC arm capacitor

**TABLE 1.** Offshore Four-Terminal HVDC Grid Parameters.

| Symbol | Value | Symbol | Value |
|---|---|---|---|
| $S_b$ | 900 MVA | $k_{p,iv}$ | 2.57 |
| $V_b^{ac}$ | 320 kV | $k_{i,iv}$ | 57.61 |
| $V_b^{dc}$ | 640 kV | $k_{p,iccz}$ | 0.83 |
| $R_g$ | 1.77 Ω | $k_{i,iccz}$ | 8.64 |
| $L_g$ | 56.3 mH | $k_{p,Pac}$ | 0.0033 |
| $R_a$ | 0.89 Ω | $k_{i,Pac}$ | 222.18 |
| $L_a$ | 84.8 mH | $k_{p,Qac}$ | 0.0033 |
| $R_{eq}$ | $R_g+R_a/2$ | $k_{i,Qac}$ | 222.18 |
| $L_{eq}$ | $L_g+L_a/2$ | $k_{p,w\Sigma z}$ | 0.54 |
| $C_{eq}$ | 0.29 $\mu$F | $k_{i,w\Sigma z}$ | 9.1 |
| $C_{dc}$ | 10 $\mu$F | droop | 0.1 |
| $C_c$ | 0.16 $\mu$F/km | $f_n$ | 50 Hz |
| $R_{c1}$ | 2.65 Ω/km | $L_{c1}$ | $6.016\times10^{-1}$ mH/km |
| $R_{c2}$ | $1.218\times10^{-1}$ Ω/km | $L_{c2}$ | $3.02\times10^{-1}$ mH/km |
| $R_{c3}$ | $1.6\times10^{-2}$ Ω/km | $L_{c3}$ | 2.8 mH/km |

energy sum and circulating current are neglected due to their relatively small impact under the assumed modulation strategy. The MMC configuration and the applied control strategy are depicted in Fig. 3, and Fig. 4, respectively. The reduced-order nonlinear SSTI MMC equations are:

$$\frac{d}{dt}i_{v,dq} = \frac{1}{L_{eq}}(v^*_{v,dq} - v_{g,dq} - R_{eq}i_{v,dq} - j\omega L_{eq}i_{v,dq}) \tag{34}$$

$$\frac{d}{dt}i_{cc,z} = \frac{1}{L_a}(\frac{v_{dc}}{2} - v^*_{cc,z} - R_a i_{cc,z}) \tag{35}$$

$$\frac{d}{dt}v_{dc} = \frac{1}{(C_{dc}+\frac{C_c}{2})}(i_c - 3i_{cc,z}) \tag{36}$$

$$\frac{d}{dt}w_{\Sigma,z} \approx -\frac{1}{2}(v^*_{v,d}i_{v,d} + v^*_{v,q}i_{v,q}) + 2v^*_{cc,z}i_{cc,z} \tag{37}$$

where $v_{v,dq}$ and $i_{v,dq}$ are the *dq*-component of the AC-side voltage and current, $v_{cc,z}$ and $i_{cc,z}$ are the zero-sequence circulating voltage and current, $v_{g,dq}$ is the *dq*-component of the equivalent grid-side voltage, $v_{dc}$ is the DC-side voltage, $i_c$ is the equivalent HVDC cable current, $w_{\Sigma,z}$ is the zero-sequence energy sum, $R_a$ and $L_a$ are the arm resistance and inductance, $R_{eq}$ and $L_{eq}$ are the equivalent grid-side and MMC arm resistance and inductance, $C_{dc}$ is the equivalent DC-side capacitance, $C_c$ is the equivalent HVDC cable capacitance, and * denotes the reference values. The reference values, derived from the MMC control loops' equations, introduce non-linearity in the above SSTI MMC equations.

The MMC SSTI control loops' equations are derived according to the control architecture shown in Fig. 3, and Fig. 4. The control strategy is based on the commonly applied cascaded control composed of inner and outer control loops with PI controllers. The PI controllers are tuned via the modulus optimum and symmetrical optimum techniques [31], where the control coefficients are presented in Table 1. The converters located at the offshore wind farms are controlled in the power mode with a zero droop coefficient. In contrast, in multiterminal configurations, the onshore grid MMCs participate in DC-side voltage control through the DC-droop mode control. The optimal linear feedback controller revising the grid control inputs can be applied as shown in Fig. 1c.

Therefore, the $x_{mmc}$, $u_{mmc}$, and $z_{mmc}$ vectors for the state-space representation of every MMC station become:

$$x_{mmc} = [i_{v,d}\ i_{v,q}\ \xi_{ivd}\ \xi_{ivq}\ i_{cc,z}\ \xi_{iccz}\ v_{dc}\ \xi_{Pac}\ \xi_{Qac}\ w_{\Sigma,z}\ \xi_{w\Sigma z}]^T \tag{38}$$

$$u_{mmc} = [v^*_{dc}\ P^*_{ac}\ Q^*_{ac}\ w^*_{\Sigma z}]^T \tag{39}$$

$$z_{mmc} = [v_{dc}]^T \tag{40}$$

where the state variable $\xi$ is associated with the PI controller's integral state at every control loop of the converter (shown in Fig. 4). It should be noted that the reference DC voltage, $v^*_{dc}$, as a control input of vector $u$, is only applicable for the MMCs with the DC-droop mode control. The number of converter state variables is $n_{mmc} = 11$, and the control inputs' number for the MMCs in the DC-droop mode control is $m_{mmc}=4$, otherwise it is $m_{mmc}=3$.

### B. STATE-SPACE REPRESENTATION OF THE HVDC CABLE

The HVDC cable is modeled based on the frequency-dependent cascaded pi-section model with parallel series branches [32] as shown in Fig. 2. This model accurately

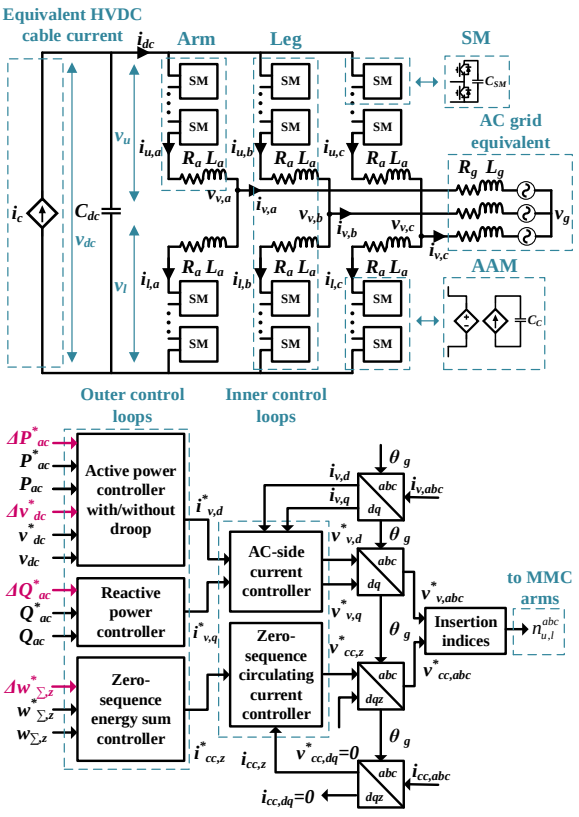


**FIGURE 3.** MMC topology and control. Delta reference values in red are from the centralized/decentralized optimal linear feedback controller.

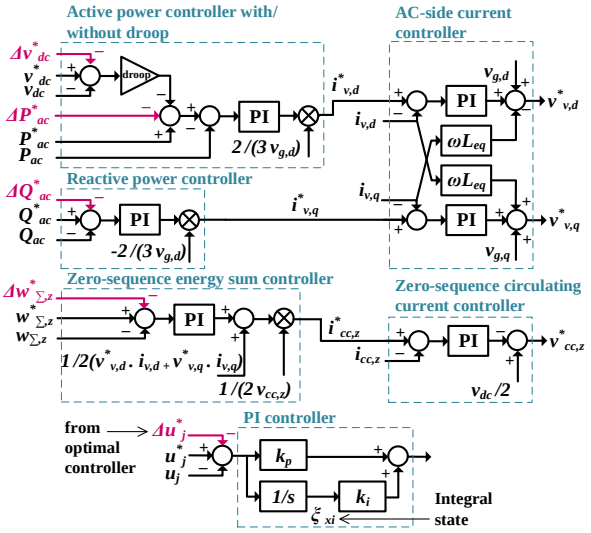


**FIGURE 4.** MMC inner and outer control loops block diagram. Delta reference values in red are from the centralized/decentralized optimal linear feedback controller.

captures the HVDC cables' damping characteristics in the frequency domain. In addition, it is suitable for state-space representation and small-signal eigenvalue stability analysis. Accordingly, the SSTI HVDC cable equations with one pi-section and three parallel series branches used in this paper are:

$$\frac{d}{dt}i_{c,i} = \frac{1}{L_{c,i}}(v_{dc1} - v_{dc2} - R_{c,i}i_{c,i}) \quad i = 1, 2, 3 \qquad (41)$$

where $R_{c,i}$ and $L_{c,i}$ are the equivalent HVDC cable resistances and inductances, which can be found through vector fitting [32] as given in Table 1. It is worth mentioning that the effect of the equivalent HVDC cable shunt capacitance, $C_c$, is considered in (36). Therefore, every HVDC cable contains three current state variables ($n_{cable} = 3$) as follows:

$$x_{cable} = [i_{c,1}\ i_{c,2}\ i_{c,3}]^T \qquad (42)$$

### C. STATE-SPACE MODEL AND SMALL-SIGNAL EIGENVALUE STABILITY ANALYSIS OF THE TEST GRID

The nonlinear SSTI state-space model of the MMC-based four-terminal HVDC grid with the expansion link $1-4$ (refer to Fig. 2) can be stated on a general form based on [33]:

$$\dot{x} = f(x, u), \quad z = g(x, u) \qquad (43)$$

with the overall $x$, $u$, and $z$ vectors:

$$x = [x_{mmc1}^T \quad x_{cable1-3}^T \quad x_{mmc3}^T \quad x_{cable1-4}^T \quad x_{mmc4}^T \quad x_{cable2-4}^T \quad x_{mmc2}^T]^T \qquad (44)$$

$$u = [u_{mmc1}^T \quad u_{mmc3}^T \quad u_{mmc4}^T \quad u_{mmc2}^T]^T \qquad (45)$$

$$z = [z_{mmc1}^T \quad z_{mmc3}^T \quad z_{mmc4}^T \quad z_{mmc2}^T]^T \qquad (46)$$

where the indices 1, 2, 3, and 4 refer to the converter stations' number, as seen in Fig. 2. Then, the total numbers of the grid state variables and control inputs are $n = 53$, and $m = 14$, respectively.

Next, time-domain simulation is required to validate the resultant SSTI state-space (SS) model's accuracy. In this regard, a circuit-based (CB) model of the HVDC grid is made using MATLAB/Simulink with the Simscape toolbox. MMC is simulated via the arm averaged model (AAM), where every converter arm is configured as a controlled voltage source with an equivalent arm capacitance (shown in Fig. 3) [30], [34]. The AAM modeling is a reliable and well-established method that considers all the converter's non-linearities and internal dynamics, ignoring the switching operation and sub-module (SM) capacitor voltage balancing algorithm. For the sake of dynamic excitation of the grid, a 10% step increase is applied to $v_{dc4}$ at $t = 0.5\ s$, and then a 50% step reduction is introduced to $P_{ac1}$ at $t = 1\ s$. The simulation results showing the dynamic response of the CB and SS models for all four converter stations for $v_{dc}$ and $P_{ac}$ waveforms are depicted in Fig. 5. The figure shows that the two models match quite well, and hence, the SSTI SS model can accurately capture the grid dynamics during the transients.

Following this, the test grid's small-signal dynamic model is obtained. For this purpose, the steady-state operating point is found by solving the equilibrium $\dot{x} = 0$ under the grid nominal working condition where the wind farms are operating at their full power capacity. Then, (43) is linearized around the resultant operating point, which is labeled as $x_0$ [33]. The matrices $A \in \mathbb{R}^{n\times n}$ and $B \in \mathbb{R}^{n\times m}$ gained from the linearized small-signal model can be incorporated into the optimal control problem formulation (10) and (28), while $C \in \mathbb{R}^{n\times n}$ is diagonal with the entries corresponding to the $z$ vector (46).

The eigenvalue stability analysis is performed to investi-

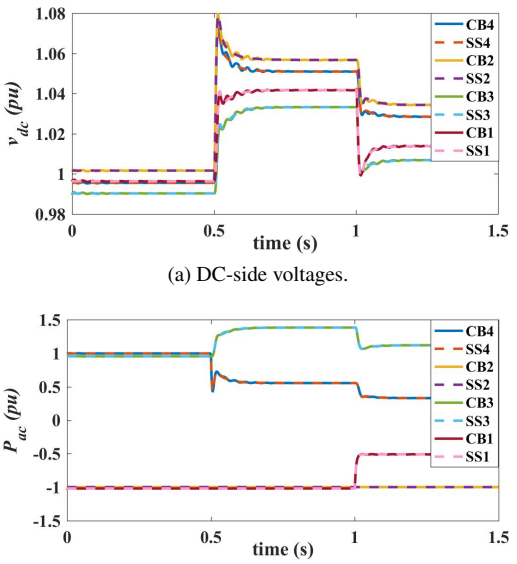


(a) DC-side voltages.

(b) AC-side active powers.

**FIGURE 5.** Time-domain verification of the SSTI state-space (SS) model and circuit-based (CB) model of the MMC-based four-terminal HVDC grid with the expansion link 1-4.

**TABLE 2.** The Most Dominant Eigenvalues and their Primary Participating States of the MMC-based Four-Terminal HVDC Grid with the Expansion Link 1-4.

| No. | Eigenvalue | Damping ratio | Oscillation frequency | Main participating states |
|---|---|---|---|---|
| $\lambda_{31,32,33}$ | –9.2 | 1 | – | $\xi_{iccz1,2,3,4}, \xi_{w\Sigma z1,2,3,4}, w_{\Sigma,z1,2,3,4}$ |
| $\lambda_{30}$ | –11.7 | 1 | – | $\xi_{iccz3,4}$ |
| $\lambda_{21,22}$ | $-15.1 \pm j\ 20.4$ | 0.59 | 3.2 HZ | $w_{\Sigma,z3,4}, \xi_{w\Sigma z3,4}, i_{c3,14}, \xi_{iccz3,4}, w_{\Sigma,z2}, \xi_{w\Sigma z2}$ |
| $\lambda_{23,24}$ | $-16.2 \pm j\ 23.7$ | 0.56 | 3.8 HZ | $w_{\Sigma,z2}, \xi_{w\Sigma z2}, \xi_{iccz2}, w_{\Sigma,z1,4}, \xi_{w\Sigma z1,4}, \xi_{iccz1,4}$ |
| $\lambda_{25,26}$ | $-16.2 \pm j\ 23.8$ | 0.56 | 3.8 HZ | $w_{\Sigma,z1}, \xi_{w\Sigma z1}, \xi_{iccz1}, w_{\Sigma,z2,3}, \xi_{w\Sigma z2,3}, \xi_{iccz2,3}$ |
| $\lambda_{27,28}$ | $-21.8 \pm j\ 15.1$ | 0.82 | 2.4 HZ | $w_{\Sigma,z3,4}, \xi_{w\Sigma z3,4}, \xi_{iccz3,4}, w_{\Sigma,z1,2}, \xi_{w\Sigma z1,2}, \xi_{iccz1,2}$ |
| $\lambda_{42,43,44,45,48,51,52,53}$ | –22.4 | 1 | – | $\xi_{ivd1,2,3,4}, \xi_{ivq1,2,3,4}$ |
| $\lambda_{29}$ | –31.9 | 1 | – | $i_{c3,14}, i_{c3,13}, \xi_{iccz3,4}, \xi_{w\Sigma z3,4}, w_{\Sigma,z3,4}$ |
| $\lambda_{20}$ | –45.7 | 1 | – | $i_{c3,24}, i_{c2,24}, w_{\Sigma,z2}, \xi_{w\Sigma z2}$ |
| $\lambda_{19}$ | –47.8 | 1 | – | $i_{c3,13}, i_{c3,14}, v_{dc1}, i_{c2,13}, w_{\Sigma,z1}, \xi_{w\Sigma z1}$ |
| $\lambda_{17,18}$ | $-116.6 \pm j\ 161.3$ | 0.59 | 25.7 HZ | $v_{dc1,2,3,4}, \xi_{Pac3,4}$ |
| $\lambda_{14,15}$ | $-158 \pm j\ 307$ | 0.46 | 48.9 HZ | $i_{c2,14}, v_{dc1,2,3,4}, \xi_{Pac3,4}$ |
| $\lambda_{1,2}$ | $-224.1 \pm j\ 1046.7$ | 0.21 | 166.7 HZ | $v_{dc3}, i_{c2,13}, v_{dc1}, \xi_{Pac3}$ |
| $\lambda_{3,4}$ | $-227.4 \pm j\ 967.4$ | 0.23 | 154.0 HZ | $i_{c2,24}, v_{dc2,4}$ |
| $\lambda_{34,35,40,41,49,50}$ | –233.7 | 1 | – | $\xi_{Pac1,2,3,4}, \xi_{Qac1,2,3,4}$ |
| $\lambda_{16}$ | –321.2 | 1 | – | $i_{c2,14}, \xi_{Pac3,4}, i_{c2,13}$ |

gate the system's dynamic properties and stability margins and corroborate the optimal controller performance. Subsequently, Table 2 lists the most dominant grid eigenvalues or modes closest to the right half-plane with their respective damping ratio, oscillatory frequency, and primary participating states with a value higher than 5% written in descending order of magnitude. Participating states are defined as the state variables contributing to their corresponding modes. As can be seen from the table, the zero-sequence energy sums and their related integral states, along with the integral states of the zero-sequence circulating current, are involved in the grid's most dominant oscillatory modes, which are specific to MMCs. This shows that analyses based on 2L-VSC [11], [12], [23], [24] should be re-evaluated, as they are unable to capture the most relevant MMC dynamics. The stability of the associated state variables is ensured by proper tuning of the converters' control parameters. The oscillatory modes of interest are the $\lambda_{17,18}$ and $\lambda_{14,15}$ because they are closest to the right half-plane with the highest participation from the $v_{dc1,2,3,4}$ and $\xi_{Pac3,4}$, which directly affect the $v_{dc1,2,3,4}$ oscillations. The states $v_{dc1,2,3,4}$ and $\xi_{Pac3,4}$ are related through the converters' droop function. The grid's eigenvalue trajectory for MMC3 and MMC4 droop coefficient variation from 0.01 to 0.2 is demonstrated in Fig. 6. The droop coefficient increase has improved the $\lambda_{14,15}$ stability margin while $\lambda_{17,18}$ has further moved towards the right half-plane, getting closer to instability. On the other hand, both $\lambda_{14,15}$ and $\lambda_{17,18}$ imaginary parts are reduced, which means a lower oscillation frequency. Therefore, it is evident that the droop function can play a pivotal role in DC-side voltage stability. Due to the trade-off between $\lambda_{14,15}$ and $\lambda_{17,18}$ when the droop coefficient increases, it is important to use an optimization strategy to readjust the droop function optimally.

Such a potential discordant effect of any droop coefficient variation on critical system eigenvalues could not be observed in our previous study of the point-to-point configuration [25], where the droop coefficient increase resulted in the progressive enhancement of the DC voltage stability margins. This reinforces the criticality of droop optimization in multiterminal applications. Hence, the optimal linear feedback controller is applied to the four-terminal HVDC grid to efficiently retune the droop gains by relocating the $\lambda_{14,15}$ and $\lambda_{17,18}$ eigenvalues to improve the DC voltage stability margins under the worst-case perturbation scenario.

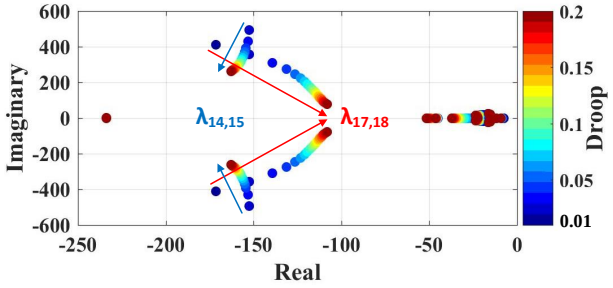


**FIGURE 6.** Eigenvalue trajectory for droop variation from 0.01 to 0.2.

## IV. SIMULATION RESULTS

The centralized and decentralized optimal control problems, (9)-(12), and (27)-(33), are solved using the YALMIP toolbox [35] of MATLAB in combination with the MOSEK solver [36], and the time-domain simulations in MATLAB/Simulink are presented in this section under different case studies. In the first example, the centralized and decentralized optimal linear feedback controllers' performance in minimizing the DC voltage oscillations under the worst-case perturbation scenario is compared through the time-domain simulations. First, the optimal controllers modify the droop control gain, and their synergistic action is assessed. Second, the droop is removed, and the optimal controllers replace the droop control function. It will be shown that the optimal controllers are capable of improving the grid DC voltage stability margins in both cases.

In the second example, the optimal DC voltage oscillation index's applicability as a support decision criterion for the placement of a new HVDC link under the wind intermittency effect is presented. It will be shown that the index can provide valuable information on HVDC cable placement.

### A. OPTIMAL LINEAR FEEDBACK CONTROLLER PERFORMANCE TEST

The four-terminal offshore HVDC grid with the expansion link 1-4 under nominal operating conditions is considered (Fig. 2). The grid state-space matrices $A \in \mathbb{R}^{n\times n}$, $B \in \mathbb{R}^{n\times m}$, and $C \in \mathbb{R}^{n\times n}$ are attained based on the derivations given in section III. Running the optimal control problem, the optimal linear feedback controller $K$, the worst initial perturbation scenario $x_{0,worst}$, and the optimal DC voltage oscillation index $\tilde{J}_{osci}$ can be obtained. The optimal controller $K$, which minimizes the DC voltage oscillations index under the worst initial perturbation scenario, can be implemented in time-domain simulations as shown in Fig. 1, 3, and 4.

#### 1) Case study I: The optimal controller performance in the presence of the grid droop control gain

A 35% step increase is applied to MMC4 reference DC-side voltage at $t = 7\,s$. The 35% step increase of the $v^*_{dc4}$ is chosen in this test case since it is the closest scenario to the worst initial perturbation scenario $x_{0,worst}$. The entries of the matrices $E_u$, and $E_x$ are one in order to define equal weight for all control inputs and state variables, except for the integral states, which are given a smaller degree of freedom. The grid waveforms for different scenarios are depicted in Fig. 7. As can be seen in Fig. 7a, the 35% step increase of the $v^*_{dc4}$ enhances the network DC-side voltages by around 20% owing to the droop control action ($droop = 0.1$). Then, the $v_{dc}$ waveforms begin to oscillate at an increasing amplitude until the system becomes unstable, as shown in Fig. 7a, 7b, 7c, and 7d. The second row of the Fig. 7 shows how the addition of a *centralized* optimal linear feedback controller can stabilize the system under such a disturbance. Due to the centralized optimal controller implementation, the system eigenvalues responsible for $v_{dc}$ oscillations ($\lambda_{1,2,3,4,14,15,17,18}$) have moved further away from the right half-plane (–185.9 $\pm\, j$ 246.4, –208.3 $\pm\, j$ 326, –264 $\pm\, j$ 970.9, and –267.3 $\pm\, j$ 1046.1), and their corresponding damping ratios have also improved (0.6, 0.54, 0.26, and 0.25, respectively). Furthermore, all entries of the found worst-case $x_{0,worst}$ are zero except for the grid DC-side voltages ($v_{dc,1,2,3,4} = 0.6, 0.1, 0.2, 0.8$). The centralized optimal linear feedback controller is a $14\times53$ matrix where the entries with the highest value can be located between a control input from one converter and a state variable in another converter. These entries are associated with the $\xi_{Pac1,2,3,4}$ and $v^*_{dc3,4}$, $\xi_{Pac1,2,3,4}$ and $w^*_{\Sigma z1,2,3,4}$, and $\xi_{Pac1,2}$ and $P^*_{ac1,2}$, which is in alignment with the results obtained from the small-signal eigenvalue stability analysis given in Table 2. Indeed, the centralized optimal controller is modifying the droop coefficient to reduce the $v_{dc}$ oscillations under the worst-case perturbation scenario.

The performance of the *decentralized* optimal linear feedback controller under the 35% step increase of the $v^*_{dc4}$ is depicted in the third row of Fig. 7. The $E^j_u$ matrices are defined such that the control inputs being confined in separate ellipsoidal constraints as follows:

$$
\begin{aligned}
&|\Delta v^*_{dc,k}| \le 1 \text{ pu}\\
&\sqrt{\Delta(P^*_{ac,k})^2 + \Delta(Q^*_{ac,k})^2} \le 1 \text{ pu}\\
&|\Delta w^*_{\Sigma z,k}| \le 1 \text{ pu} \quad k = 1,2,3,4
\end{aligned}
$$

On the other hand, the $E^i_x$ matrices are assigned values so that the state variables can vary within a reasonable range and be modified based on the desired offshore HVDC grid codes and standards. A 0.15 pu limit is borrowed from the Commission Regulation (EU) 2016/1447 network code [37] on the required AC voltage ranges for the HVDC converter to remain connected at the connection point to the network. The DC voltages, together with other state variables' limit, are all set to 0.15 pu except for the state variables' integral parameters and the $w_{\Sigma z}$, which is proportional to the square of the sum of the arm capacitor voltages:

$$
\begin{aligned}
&|\Delta i_{v,k}| = \sqrt{\Delta i^2_{vd,k} + \Delta i^2_{vq,k}} \le 0.15 \text{ pu}\\
&|\Delta \xi_{iv,k}| = \sqrt{\Delta \xi^2_{ivd,k} + \Delta \xi^2_{ivq,k}} \le \varepsilon\\
&|\Delta i_{cz,k}| \le 0.15 \text{ pu} \quad |\Delta \xi_{icz,k}| \le \varepsilon \quad |\Delta v_{dc,k}| \le 0.15 \text{ pu}\\
&\sqrt{\Delta \xi^2_{Pac,k} + \Delta \xi^2_{Qac,k}} \le \varepsilon\\
&|\Delta w_{\Sigma z,k}| \le 0.5 \text{ pu} \quad |\Delta \xi_{w\Sigma z,k}| \le \varepsilon \quad \varepsilon = 10^{-5}\\
&\sqrt{\Delta i^2_{c1,kk} + \Delta i^2_{c2,kk} + \Delta i^2_{c3,kk}} \le 0.15 \text{ pu} \quad k = 1,2,3,4
\end{aligned}
$$

The dominant entries of the decentralized optimal controller matrix in charge of DC voltage oscillations' minimization are associated with the following pairs: $v^*_{dc3,4}$ and $\xi_{ivd3,4}$, $v^*_{dc3,4}$ and $\xi_{Pac3,4}$, $P^*_{ac1,2,3,4}$ and $\xi_{ivd1,2,3,4}$, $P^*_{ac1,2,3,4}$ and $\xi_{Pac1,2,3,3,4}$, and $w^*_{\Sigma z1,2,3,4}$ and $\xi_{Pac1,2,3,3,4}$. This result is in accordance with the block-diagonal configuration of the decentralized optimal controller matrix, where all the inter-converter entries are zero. Accordingly, all the $v_{dc}$ related eigenvalues are pushed further away from the right half-plane (–238 $\pm\, j$ 237, –297 $\pm\, j$ 987, and –298 $\pm\, j$ 972) and their corresponding damping ratios become 0.71, 0.29, and 0.29, respectively. Furthermore, the worst initial perturbation scenario under the decentralized optimal controller implementation is obtained at the boundary of the state variables' limit thanks to the state variables' decoupled confinement in separate ellipsoids.

As can be seen from Fig. 7, the centralized optimal controller has stabilized the system by slightly reducing the grid DC-side voltages and increasing some grid AC-side active powers. As a result, the converters' zero-sequence energy sum have changed to keep the grid power balanced. In contrast, the decentralized optimal controller has kept the

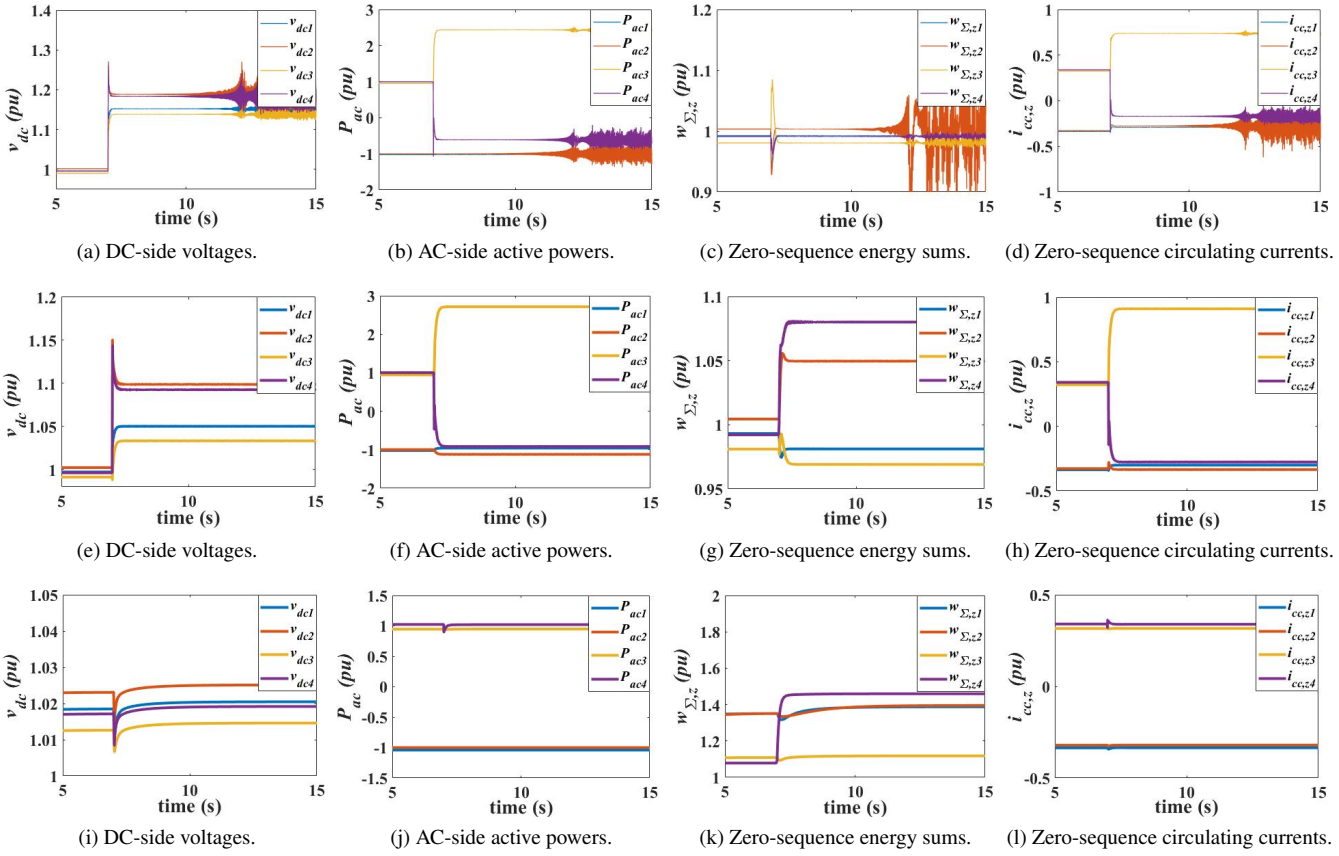


**FIGURE 7.** MMCs' waveforms after applying a 35% step increase to the MMC4 DC-side voltage at $t = 7\ s$: (first row: a, b, c, & d) without optimal linear feedback controller, (second row: e, f, g, & h) centralized optimal linear feedback controller with droop, (third row: i, j, k, & l) decentralized optimal linear feedback controller with droop.

grid DC-side voltages and AC-side active powers almost constant while varying the converters' zero-sequence energy sum and diverting the variations to the arm capacitors to meet the grid control inputs' and the state variables' constraints. It is worth mentioning that the grid power-sharing is outside of this paper's scope, but it can be handled by the grid secondary control.

### 2) Case study II: The optimal controller performance in the absence of the grid droop control gain

The droop control gain of the grid onshore converters MMC3 and MMC4 is set to zero so that the system becomes unstable with an eigenvalue on the right half-plane ($\lambda = +0.34$). To investigate whether the optimal controller can handle the droop control task and balance the grid power, a 15% step reduction is applied to $P^*_{ac4}$ at $t = 17\ s$. This scenario estimates the found worst-case perturbation under the centralized optimal controller implementation. The simulation results are shown in Fig. 8. Both the centralized and decentralized optimal controllers can substitute the droop control function under the steady-state condition and after the dynamics and move the system eigenvalues away from the right half-plane. The optimal controller matrix dominant entries in both the centralized and decentralized optimal controllers are associated with the $\xi_{Pac1,2,3,4}$ (integral state of the AC-side active powers) and $w^*_{\Sigma z,1,2,3,4}$ (reference zero-sequence energy sums), and $\xi_{Pac1,2,3,4}$ (integral state of the AC-side active powers) and $P^*_{ac1,2,3,4}$ (reference AC-side active powers) pairs, with all the inter-converter entries equal to zero in the decentralized one. The two methods' apparent difference is the role of the converters' zero-sequence energy sum in the decentralized optimal controller. Namely, the decentralized optimal controller keeps the grid DC-side voltages and AC-side active powers relatively unchanged after the worst initial perturbation scenario by varying the zero-sequence energy sum within the constraints and diverting the variations to the MMC arm capacitors. The relation between the MMC4 zero-sequence energy sum (shown in Fig. 8g) and the sum of the upper arm capacitor voltages is depicted in Fig. 9 as an example. It is assumed that the converter arm capacitors have sufficient capacity to accept such overvoltage under the worst-case perturbation scenario. This can be achieved by either increasing the number of MMC submodules or increasing the voltage rating of the submodule capacitors.

In summary, both the centralized and decentralized optimal linear feedback controllers can guarantee sufficient DC voltage stability margins by relocating the $\lambda_{14,15}$ and $\lambda_{17,18}$ eigenvalues in the droop controller's absence under

This article has been accepted for publication in a future issue of this journal, but has not been fully edited. Content may change prior to final publication. Citation information: DOI 10.1109/ACCESS.2021.3096291, IEEE Access



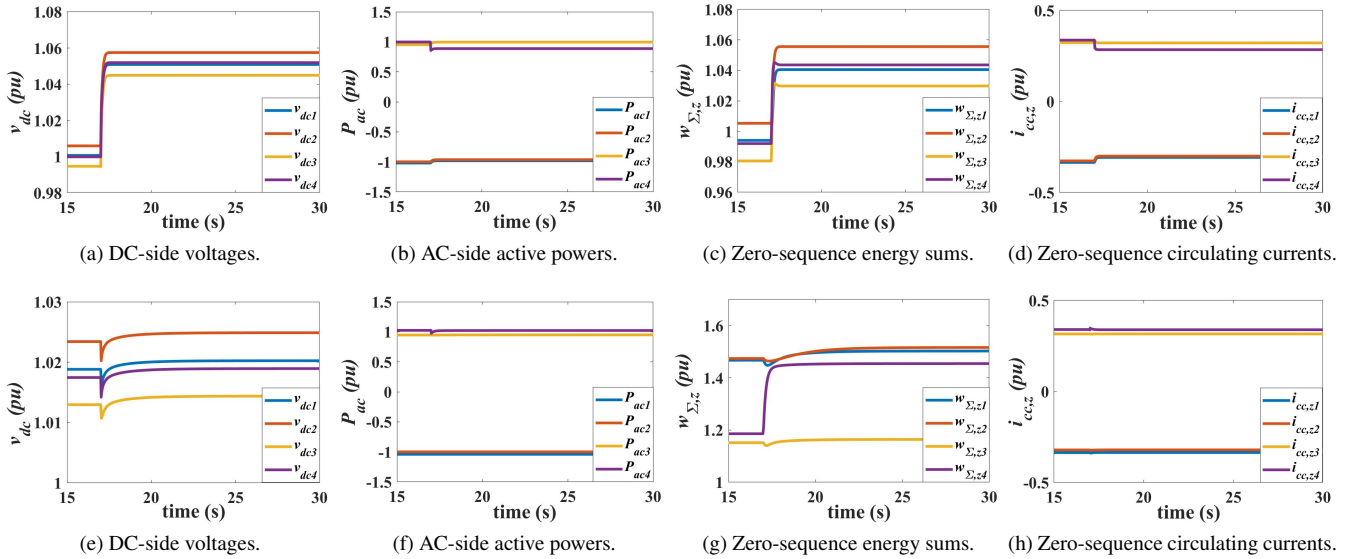


**FIGURE 8.** MMCs' waveforms after applying a 15% step reduction to the MMC4 AC-side active power at $t = 17$: (first row: a, b, c, & d) centralized linear feedback controller without droop, (second row: e, f, g, & h) decentralized linear feedback controller without droop.

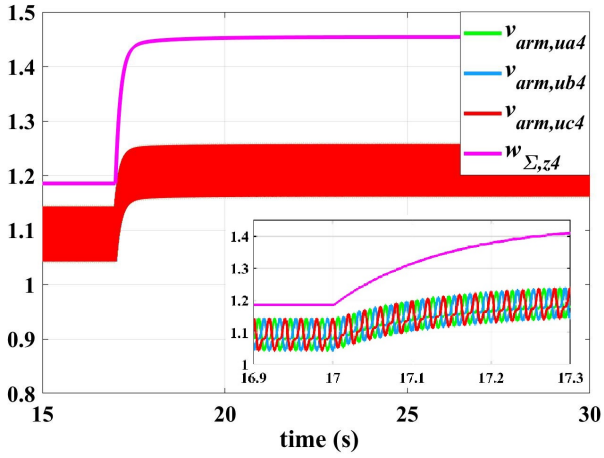


**FIGURE 9.** MMC4 zero-sequence energy sum and sum of the upper arm capacitor voltages after applying a 15% step reduction to the MMC4 AC-side active power at $t = 17$.

the worst initial perturbation scenario. The droop controller alone would not ensure such stability. However, through the addition of the optimal controller in the droop control gain's presence, the synergy between them can be exploited to minimize the DC voltage oscillations with larger stability margins. Besides, the possibility of having the optimal controller work in the presence of the droop control gain may pave the way to its selective action, i.e., the possibility of being activated when worst-case conditions occur.

### B. OPTIMAL DC VOLTAGE OSCILLATION INDEX APPLICATION

The optimal DC voltage oscillation index as a potential decision criterion can be used to identify the route prone to minimum DC voltage oscillations for connecting the two independent offshore point-to-point HVDC grids while considering the wind intermittency effect. The optimal DC voltage oscillation index is dependent on the offshore converters' operating points, around which (43) is linearized. These operating points are representative of different wind power extractions and correspondingly varied wind speed scenarios. The *Reanalysis* dataset is used as a basis to extract average wind speed time series for the two offshore sites [38]. Further analysis is performed exploiting the histograms of hourly wind speed and the normalized mean wind power curves for the two offshore locations to quantify the total wind power production of the subsequent four-terminal grid [24]. Table 3 shows the probability of simultaneous generation of normalized power in four different ranges (0-0.25 pu, 0.25-0.5 pu, 0.5-0.75 pu, and 0.75-1 pu) at the two offshore sites. Namely, the probability of 0.09 at the intersection of 0.75-1 pu normalized power, for instance, can be interpreted as a 9% probability for the two wind farms to generate electricity in the range of 0.75-1 pu simultaneously. Wind farm operating points are designated to be the average of each normalized power range shown in Table 3. Accordingly, the oscillation indices are calculated for 16 different scenarios for every added HVDC cable ($1-2$, $1-4$, $2-3$, and $3-4$). The oscillation indices at the nominal operating condition and the average DC voltage oscillation indices are given in Table 4 for the centralized and decentralized linear controllers with the droop and the four HVDC cable options. The average DC voltage oscillation indices are calculated as the sum of all the products between the optimal DC voltage oscillation indices and their corresponding event probability given in Table 3. The optimal HVDC route with minimum $\tilde{J}_{osci}$ at every scenario is marked in boldface.

It can be seen from Table 4 that the added HVDC link $1-2$ with the least length is the optimal solution in all

**TABLE 3.** Probability of Simultaneous Generation of Normalized Power at Johan-Sverdrup and BorWin1 Locations.

| Normalized power ranges (pu) | | BorWin1 | | | |
|---|---|---|---|---|---|
| | | 0 – 0.25 | 0.25 – 0.5 | 0.5 – 0.75 | 0.75 – 1 |
| Johan – Sverdrup | 0 – 0.25 | 0.22 | 0.09 | 0.06 | 0.04 |
| | 0.25 – 0.5 | 0.07 | 0.05 | 0.04 | 0.04 |
| | 0.5 – 0.75 | 0.04 | 0.04 | 0.04 | 0.05 |
| | 0.75 – 1 | 0.03 | 0.04 | 0.05 | 0.09 |

**TABLE 4.** Optimal DC Voltage Oscillation Index at Nominal Condition Versus Average Optimal DC Voltage Oscillation Index under the Centralized and Decentralized Optimal Linear Feedback Controllers with Droop.

| Added HVDC link | Length (km) | Centralized optimal controller | | Decentralized optimal controller | |
|---|---|---|---|---|---|
| | | $\tilde{J}_{osci}$ at nominal condition | Average $\tilde{J}_{osci}$ | $\tilde{J}_{osci}$ at nominal condition | Average $\tilde{J}_{osci}$ |
| 1 – 2 | 600 | **32.0*** | **34.7*** | **14.3*** | **13.2*** |
| 1 – 4 | 750 | 37.9 | 40.9 | 17.4 | 15.4 |
| 2 – 3 | 650 | 35.2 | 38.1 | 15.5 | 13.8 |
| 3 – 4 | 800 | 41.2 | 44.5 | 25.3 | 22.6 |

four different scenarios. The HVDC cable stability margin is expected to increase with the cable length [39]. Hence, the results suggest that the optimal controller's effectiveness in the DC voltage oscillations' minimization increases at lower stability margin conditions. Namely, the lower the cable length, the lower the optimal DC voltage oscillation index. On the other hand, the $\tilde{J}_{osci}$ at nominal condition, and the average $\tilde{J}_{osci}$ lead to the same optimal result. That is to say that the wind intermittency does not affect the HVDC cable placement with minimum DC voltage oscillations in this case. However, in real-life situations, converters and HVDC cables from various suppliers can have different specifications and parameters. Due to this variety, the average $\tilde{J}_{osci}$ may result in a different optimal HVDC cable route than only considering the nominal operating condition [24].

From another perspective, the optimal DC voltage oscillation indices can be weighted together with other decision criteria by grid expansion planners. For instance, in the decentralized case, the second optimal solution (link 2-3) based on the average $\tilde{J}_{osci}$ is quite close to the first one (link 1-2), while looking at the $\tilde{J}_{osci}$ at nominal condition, the difference is more noticeable. In fact, the second optimal solution is almost as good as the first one that would not have emerged from the nominal condition analysis. Such insight could also be valuable for grid expansion planners while assessing all design criteria together.

## V. CONCLUSION

In this paper, the centralized and decentralized optimal linear feedback controllers were presented to reduce DC voltage oscillations under the worst-case perturbation scenario in an offshore four-terminal HVDC grid. The grid configuration was based on the MMC. It was observed that the distinct MMC eigenvalues associated with the zero-sequence circulating current and zero-sequence energy sum state variables and their integral parameters were the closest to the instability region. Therefore, the simplified analyses based on 2-level VSCs in contrast with MMCs are not sufficient for the grid state-space model and stability studies. The stability margins of the MMC state variables can be improved by proper tuning of the control parameters.

It is observed from the eigenvalue stability analysis that the two eigenvalue pairs responsible for the DC voltage oscillations are related to the grid DC-side voltage and the integral state of the AC-side active power, which are connected through the droop control gain. The eigenvalue trajectory study for droop variations in the four-terminal grid depicted a trade-off between these two eigenvalue pairs. An eigenvalue pair's stability margins have improved, while the other pair has become more prone to instability by further moving towards the right half-plane. To this end, an optimization strategy is beneficial to optimally readjust the droop gains to improve the DC voltage stability margins.

The time-domain simulations showed that the centralized and decentralized optimal linear feedback controllers could improve the DC voltage stability margins under the worst initial perturbation scenario when implemented either in the presence or absence of the droop control gain. In the former case, better performance is obtained because the synergies between the optimal controller and the droop control function can result in the minimization of the DC voltage oscillations with larger stability margins. Moreover, unlike the droop controller, the centralized and decentralized optimal linear feedback controllers can inherently satisfy the control inputs' and state variables' constraints.

An apparent difference is noted from the centralized and decentralized optimal controllers' response to disturbances based on the time-domain simulations. The converters' zero-sequence energy sum's control plays a pivotal role in the performance of the decentralized optimal controller. Namely, the controller maintains the grid DC-side voltages and AC-side active powers relatively constant after the worst-case scenario by diverting the perturbations to the MMC arm capacitors resulting in the variation of the converters' zero-sequence energy sum. Hence, it may rely on an increased number of the MMC sub-modules or a higher voltage rating of the MMC sub-module capacitors.

As a further contribution, the optimal DC voltage oscillation index was applied as a potential decision support criterion for the placement of a new HVDC cable between two independent point-to-point offshore HVDC grids while considering the wind intermittency effect. The lowest oscillation index was obtained for the HVDC cable with the lowest length.

Finally, one potential extension of the proposed method could be to investigate the minimization of DC voltage oscillations together with the angular swings of the synchronous generator in hybrid AC/DC networks to expand the range of applicability of the methodology.

## REFERENCES


[1] W. Zappa, M. Junginger, and M. van den Broek, "Is a 100% renewable european power system feasible by 2050?" *Applied Energy*, vol. 233-234, pp. 1027–1050, 2019. [Online]. Available: https://www.sciencedirect.com/science/article/pii/S0306261918312790

[2] Y. Zhang, C. Klabunde, and M. Wolter, "Frequency-coupled impedance modeling and resonance analysis of dfig-based offshore wind farm with hvdc connection," *IEEE Access*, vol. 8, pp. 147 880–147 894, 2020.

[3] B. Zhang and H. Nademi, "Modeling and harmonic stability of mmc-hvdc with passive circulating current filters," *IEEE Access*, vol. 8, pp. 129 372–129 386, 2020.

[4] A. Dekka, B. Wu, R. L. Fuentes, M. Perez, and N. R. Zargari, "Evolution of topologies, modeling, control schemes, and applications of modular multilevel converters," *IEEE Journal of Emerging and Selected Topics in Power Electronics*, vol. 5, no. 4, pp. 1631–1656, 2017.

[5] A. Elahidoost and E. Tedeschi, "Expansion of offshore hvdc grids: An overview of contributions, status, challenges and perspectives," in *2017 IEEE 58th International Scientific Conference on Power and Electrical Engineering of Riga Technical University (RTUCON)*, 2017, pp. 1–7.

[6] J. Gorenstein Dedecca, S. Lumbreras, A. Ramos, R. A. Hakvoort, and P. M. Herder, "Expansion planning of the north sea offshore grid: Simulation of integrated governance constraints," *Energy Economics*, vol. 72, pp. 376–392, 2018. [Online]. Available: https://www.sciencedirect.com/science/article/pii/S0140988318301622

[7] W. Wang and M. Barnes, "Power flow algorithms for multi-terminal vsc-hvdc with droop control," *IEEE Transactions on Power Systems*, vol. 29, no. 4, pp. 1721–1730, 2014.

[8] G. Pinares and M. Bongiorno, "Analysis and mitigation of instabilities originated from dc-side resonances in vsc-hvdc systems," *IEEE Transactions on Industry Applications*, vol. 52, no. 4, pp. 2807–2815, 2016.

[9] A. A. Taffese, A. G. Endegnanew, S. D'Arco, and E. Tedeschi, "Power oscillation damping with virtual capacitance support from modular multilevel converters," *IET Renewable Power Generation*, vol. 14, no. 5, pp. 897–905, 2020.

[10] W. Xiang, S. Yang, L. Xu, J. Zhang, W. Lin, and J. Wen, "A transient voltage-based dc fault line protection scheme for mmc-based dc grid embedding dc breakers," *IEEE Transactions on Power Delivery*, vol. 34, no. 1, pp. 334–345, 2019.

[11] E. Prieto-Araujo, A. Egea-Alvarez, S. Fekriasl, and O. Gomis-Bellmunt, "Dc voltage droop control design for multiterminal hvdc systems considering ac and dc grid dynamics," *IEEE Transactions on Power Delivery*, vol. 31, no. 2, pp. 575–585, 2016.

[12] M. N. Ambia, K. Meng, W. Xiao, A. Al-Durra, and Z. Y. Dong, "Adaptive droop control of multi-terminal hvdc network for frequency regulation and power sharing," *IEEE Transactions on Power Systems*, vol. 36, no. 1, pp. 566–578, 2021.

[13] X. Chen, L. Wang, H. Sun, and Y. Chen, "Fuzzy logic based adaptive droop control in multiterminal hvdc for wind power integration," *IEEE Transactions on Energy Conversion*, vol. 32, no. 3, pp. 1200–1208, 2017.

[14] S. D. Tavakoli, E. Sánchez-Sánchez, E. Prieto-Araujo, and O. Gomis-Bellmunt, "Dc voltage droop control design for mmc-based multiterminal hvdc grids," *IEEE Transactions on Power Delivery*, vol. 35, no. 5, pp. 2414–2424, 2020.

[15] Z. Zhuo, N. Zhang, J. Yang, C. Kang, C. Smith, M. J. O'Malley, and B. Kroposki, "Transmission expansion planning test system for ac/dc hybrid grid with high variable renewable energy penetration," *IEEE Transactions on Power Systems*, vol. 35, no. 4, pp. 2597–2608, 2020.

[16] M. Moradi-Sepahvand and T. Amraee, "Hybrid ac/dc transmission expansion planning considering hvac to hvdc conversion under renewable penetration," *IEEE Transactions on Power Systems*, vol. 36, no. 1, pp. 579–591, 2021.

[17] H. Xie, Z. Bie, and G. Li, "Reliability-oriented networking planning for meshed vsc-hvdc grids," *IEEE Transactions on Power Systems*, vol. 34, no. 2, pp. 1342–1351, 2019.

[18] A. A. Eajal, A. H. Yazdavar, E. F. El-Saadany, and K. Ponnambalam, "On the loadability and voltage stability of islanded ac–dc hybrid microgrids during contingencies," *IEEE Systems Journal*, vol. 13, no. 4, pp. 4248–4259, 2019.

[19] J. L. Rueda, W. H. Guaman, J. C. Cepeda, I. Erlich, and A. Vargas, "Hybrid approach for power system operational planning with smart grid and small-signal stability enhancement considerations," *IEEE Transactions on Smart Grid*, vol. 4, no. 1, pp. 530–539, 2013.

[20] J. Qiu, Z. Y. Dong, J. Zhao, Y. Xu, F. Luo, and J. Yang, "A risk-based approach to multi-stage probabilistic transmission network planning," *IEEE Transactions on Power Systems*, vol. 31, no. 6, pp. 4867–4876, 2016.

[21] H. Ergun, B. Rawn, R. Belmans, and D. Van Hertem, "Stepwise investment plan optimization for large scale and multi-zonal transmission system expansion," *IEEE Transactions on Power Systems*, vol. 31, no. 4, pp. 2726–2739, 2016.

[22] ——, "Technology and topology optimization for multizonal transmission systems," *IEEE Transactions on Power Systems*, vol. 29, no. 5, pp. 2469–2477, 2014.

[23] A. Elahidoost, L. Furieri, E. Tedeschi, and M. Kamgarpour, "Optimizing hvdc grid expansion and control for enhancing dc stability," in *2018 Power Systems Computation Conference (PSCC)*, 2018, pp. 1–7.

[24] ——, "Reducing hvdc network oscillations considering wind intermittency through optimized grid expansion decision," in *2018 IEEE Energy Conversion Congress and Exposition (ECCE)*, 2018, pp. 2683–2690.

[25] A. Elahidoost and E. Tedeschi, "Control optimization of the offshore hvdc grid based on modular multilevel converter for improving dc voltage stability," in *The Renewable Energy & Power Quality Journal (RE&PQJ)*, vol. 18, no. 273, 2020, pp. 207–212.

[26] A. Fuchs and M. Morari, "Actuator performance evaluation using lmis for optimal hvdc placement," in *2013 European Control Conference (ECC)*, 2013, pp. 1529–1534.

[27] S. Boyd, L. EL Ghaoui, E. Feron, and V. Balakrishnan, *Linear Matrix Inequalities in System and Control Theory*. Philadelphia: SIAM Studies in Applied Mathematics, 1994, vol. 15.

[28] W. Leterme, N. Ahmed, J. Beerten, L. Ängquist, D. V. Hertem, and S. Norrga, "A new hvdc grid test system for hvdc grid dynamics and protection studies in emt-type software," in *11th IET International Conference on AC and DC Power Transmission*, 2015, pp. 1–7.

[29] Government.no, "Norway opens offshore areas for wind power," 2020. [Online]. Available: "https://www.regjeringen.no/en/aktuelt/norway-opens-offshore-areas-for-wind-power/id2705986/"

[30] G. Bergna-Diaz, J. A. Suul, and S. D'Arco, "Energy-based state-space representation of modular multilevel converters with a constant equilibrium point in steady-state operation," *IEEE Transactions on Power Electronics*, vol. 33, no. 6, pp. 4832–4851, 2018.

[31] S. Sanchez, G. Bergna, and E. Tedeschi, "Tuning of control loops for grid-connected modular multilevel converters under a simplified port representation for large system studies," in *2017 Twelfth International Conference on Ecological Vehicles and Renewable Energies (EVER)*, 2017, pp. 1–8.

[32] J. Beerten, S. D'Arco, and J. A. Suul, "Frequency-dependent cable modelling for small-signal stability analysis of vsc-hvdc systems," *IET Generation, Transmission Distribution*, vol. 10, no. 6, pp. 1370–1381, 2016.

[33] P. Kundur, *Power System Stability and Control*. New York, NY, USA: McGraw-Hill, 1994.

[34] L. Harnefors, A. Antonopoulos, S. Norrga, L. Angquist, and H. Nee, "Dynamic analysis of modular multilevel converters," *IEEE Transactions on Industrial Electronics*, vol. 60, no. 7, pp. 2526–2537, 2013.

[35] J. Lofberg, "Yalmip : a toolbox for modeling and optimization in matlab," in *2004 IEEE International Conference on Robotics and Automation (IEEE Cat. No.04CH37508)*, 2004, pp. 284–289.

[36] E. D. Andersen and K. D. Andersen, *The Mosek Interior Point Optimizer for Linear Programming: An Implementation of the Homogeneous Algorithm*. Boston, MA: Springer US, 2000, pp. 197–232. [Online]. Available: https://doi.org/10.1007/978-1-4757-3216-0_8

[37] entsoe.eu, "Commission regulation (eu) 2016/1447 of 26 august 2016 establishing a network code on requirements for grid connection of high voltage direct current systems and direct current-connected power park modules," 2016. [Online]. Available: "http://data.europa.eu/eli/reg/2016/1447/oj"

[38] H. Svendsen, "Hourly wind and solar energy time series from reanalysis dataset," SINTEF Energi AS, Norway, Tech. Rep., 2017. [Online]. Available: http://hdl.handle.net/11250/2468143

[39] W. Wu, A. Luo, Y. Chen, Y. Dong, L. Zhou, X. Zhou, L. Yang, Z. He, Q. Xu, and X. Huang, "Dc impedance modeling, stability analysis and active stabilization of the vsc-hvdc system," in *IECON 2017 - 43rd Annual Conference of the IEEE Industrial Electronics Society*, 2017, pp. 4891–4896.

This article has been accepted for publication in a future issue of this journal, but has not been fully edited. Content may change prior to final publication. Citation information: DOI 10.1109/ACCESS.2021.3096291, IEEE Access



ATOUSA ELAHIDOOST (M'16) received her M.Sc. degree in electronics engineering from the Azad University of Central Tehran Branch (IAUCTB), Tehran, Iran, in 2011, and her M.Sc. degree in electric power engineering from the Norwegian University of Science and Technology (NTNU), Trondheim, Norway, in 2016. She is currently pursuing a Ph.D. degree with the Department of Electric Power Engineering at NTNU, where she focuses on the optimal control of the offshore multiterminal HVDC grids.

From 2006 to 2009, she was an Electrical Engineer with Pars Tableau Switchgear Systems, where she worked on designing power distribution control systems (PDCS) and power management systems (PMS). She then joined Energy Industries Engineering and Design (EIED), where she was an electrical engineering consultant until 2013. She is currently with NTNU, and her main research interests are modeling and control of the power electronic conversion systems with the penetration of renewables, such as solar and wind energy.

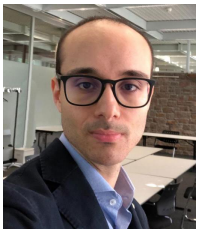

LUCA FURIERI received his Ph.D. degree from ETH Zurich, Switzerland, in 2020, and his B.Sc. and M.Sc. degrees in Automation Engineering from the University of Bologna, Italy, in 2014 and 2016, respectively. He is currently a Postdoctoral scientist at the Automatic Control Laboratory, EPFL Lausanne, Switzerland.

His research interests lie in the broad areas of learning and optimal control for distributed decision-making and safety-critical applications.

Dr. Furieri was the recipient of the O. Hugo Schuck Best Paper Award in 2018 and was a finalist for the Best Student Paper Award at the 2019 European Control Conference (ECC).

MARYAM KAMGARPOUR holds a Doctor of Philosophy in Engineering from the University of California, Berkeley, CA, USA, in 2011, and a Bachelor of Applied Science from University of Waterloo, Waterloo, ON, Canada, in 2005.

She was an Assistant Professor, ETH Zürich. She is currently an Assistant Professor of Electrical and Computer Engineering with the University of British Columbia, Vancouver, whose research focuses on advancing a fundamental understanding of multiagent decision-making in uncertain and dynamic environments. Toward this goal, she develops algorithms for safe optimization and learning, game theory and distributed control, as well as stochastic and data-driven optimization and control. Her theoretical research is driven by control challenges arising in intelligent transportation networks, rescue robotics, and power grid systems.

Dr. Kamgarpour was the recipient of NASA High Potential Individual Award and NASA Excellence in Publication Award for her work on air traffic control systems in collaboration with NASA Ames Research Center and the European Union (ERC) Starting Grant for her work on multiagent decision-making and control for power systems.

ELISABETTA TEDESCHI received her M.Sc. degree (with honors) in electrical engineering and the Ph.D. degree in industrial engineering from the University of Padova, Italy, in 2005 and 2009, respectively.

From 2009 to 2011, she was a postdoctoral researcher at the Norwegian University of Science and Technology (NTNU), working on the grid integration of offshore renewable energies. Having received a Marie Curie Fellowship, she was a Researcher at Tecnalia, Spain, from 2011 to 2013, where she worked as a principal investigator in the FP7-Sea2grid Project, related to the storage needs for the grid integration of wave energy converters. From 2013 to 2014, she was Research Scientist at SINTEF Energy and Adjunct Associate Professor at NTNU. In 2014, she became Full Professor within the offshore grid at NTNU. Since 2020 she is also Full Professor at the Department of Industrial Engineering of the University of Trento, Italy. She has a core competence in the design and control of energy conversion and transmission and distribution systems, with a focus on offshore energy, and power-quality issues. She has led and/or contributed to more than 15 national and international scientific projects and she is the author or co-author of two book chapters and more than 100 journals and conference papers in the field of marine energy and energy conversion systems.